available at www.sciencedirect.com

ScienceDirect

journal homepage: www.elsevier.com/locate/chnjc

Article

Bimetallic Cr-In/H-SSZ-13 for selective catalytic reduction of nitric oxide by methane

Jun Yang [a], Yupeng Chang [a], Weili Dai [a], Guangjun Wu [a], Naijia Guan [a,b], Landong Li [a,b,*]

[a] *School of Materials Science and Engineering & National Institute for Advanced Materials, Nankai University, Tianjin 300071, China*

[b] *Key Laboratory of Advanced Energy Materials Chemistry of the Ministry of Education, Collaborative Innovation Center of Chemical Science and Engineering, Nankai University, Tianjin 300071, China*

ARTICLE INFO

Article history:
Received 7 February 2018
Accepted 7 March 2018
Published 5 May 2018

Keywords:
Selective catalytic reduction
Nitric oxide
Methane
Cr-In/H-SSZ-13
Bimetallic catalyst

ABSTRACT

Bimetallic Cr-In/H-SSZ-13 zeolites were prepared by wet impregnation and investigated for selective catalytic reduction of nitric oxide by methane (CH_4-SCR). Reduction-oxidation treatments led to close contact and interaction between Cr and In species in these zeolites, as revealed by transmission electron microscopy and X-ray photoelectron spectroscopy. Compared to monometallic Cr/H-SSZ-13 and In/H-SSZ-13, the bimetallic catalyst system exhibited dramatically enhanced CH_4-SCR performance, i.e., NO conversion greater than 90% and N_2 selectivity greater than 99% at 550 °C in the presence of 6% H_2O under a high gas hourly space velocity of 75 000 /h. The bimetallic Cr-In/H-SSZ-13 showed very good stability in CH_4-SCR with no significant activity loss for over 160 h. Catalytic data revealed that CH_4 and NO were activated on the In and Cr sites of Cr-In/H-SSZ-13, respectively, both in the presence of O_2 during CH_4-SCR.

1. Introduction

Nitrogen oxides derived from boilers, engines, and power plants contribute to the formation of photochemical smog and acid rain and are harmful to human health [1]. The selective catalytic reduction of nitrogen oxides (NO and NO_2) by hydrocarbons (HC-SCR) is a promising strategy for the post-treatment of nitrogen oxides in excess oxygen, and CH_4 is an attractive reductant because of its low cost and easy availability in natural gas power plants. In China, CH_4-SCR is now attracting particular interest in the move to replace coal with natural gas as a raw material for urban power plants. However, because of its chemical inertness, methane is difficult to activate, which remains a key problem in the CH_4-SCR [2–5]. However, NO oxidation, the role of which is still unclear and seems dependent on the catalysts employed [6], is an important step in the CH_4-SCR.

Zeolites, known as microporous crystalline aluminosilicates, can be directly used as catalysts [7,8] and are more frequently used as catalyst supports [9] in SCR. Transition-metal-modified zeolites have been extensively investigated for CH_4-SCR in past decades [10–33]. Among them, In-modified zeolites appear to be most active monometallic catalysts for CH_4-SCR because of the effective activation of CH_4 by In species [22–29,32]. It was claimed that methane can be activated on In_2O_3 sites to generate oxygenates, which then react with nitrate to generate N_2 [22]. Alternatively, the H_2NCO intermediate formed by the reaction between NO_2 and partially oxidized methane on intrazeolite InO^+ sites was proposed to be the actual NO reductant in the CH_4-SCR [23]. To improve the CH_4-SCR activity, second

* Corresponding author. Tel/Fax: +86-22-23500341; E-mail: lild@nankai.edu.cn
This work was supported by the National Natural Science Foundation of China (21773127, 21722303, 21421001) and the 111 Project (B18030).
DOI: 10.1016/S1872-2067(18)63054-2 | http://www.sciencedirect.com/science/journal/18722067 | Chin. J. Catal., Vol. 39, No. 5, May 2018

transition metals, e.g., Pd [13,14], Co [3,19], and Ce [20], were introduced to In-zeolites, and the major role of the second transition metals was proposed to promote the oxidative activation of NO [3,14,16,20]. For example, the cobalt oxide clusters in Co-In/HZSM-5 showed a positive effect on the oxidation of NO to NO_2, which promoted the CH_4-SCR [3]. Similarly, palladium in Pd-In/H-ZSM-5 promoted the oxidation of NO and increased the formation of the activated nitrate species, while In^+/InO^+ sites suppressed the formation of less reactive isocyanate and nitrile species [14].

In this work, we aimed to develop an efficient catalyst for the CH_4-SCR, i.e., achieving good activity and stability in the presence of excess H_2O and under high space velocity conditions. H-SSZ-13, a high-silica zeolite with a CHA topology, was first used as a catalytic support for CH_4-SCR because of its high stability against framework dealumination. Bimetallic Cr-In/H-SSZ-13 was optimized and its structure-activity relationship in the CH_4-SCR was analyzed.

2. Experimental

2.1. Catalyst preparation

All the chemical reagents employed in this study were of analytical grade from Alfa Aesar and used as received without further purification. Commercial zeolites in their H form with similar Si/Al ratios of 24, i.e., H-SSZ-13, H-ZSM-5, and H-beta, as well as amorphous SiO_2 (surface area of 210 m^2/g) were used as supports, and metal modifiers were introduced via wet impregnation. In a typical process, the zeolite support was immersed in a solution containing the desired amount of indium nitrate and chromium nitrate and stirred at room temperature for 24 h. Subsequently, the solvent of the slurry was removed in a rotary evaporator at 80 °C, and the residue was dried in an oven at 80 °C for 12 h. The obtained solid sample was calcined in Ar at 550 °C for 2 h, reduced in 10% H_2/Ar at 450 °C for 1 h, and oxidized in 10% O_2/Ar at 450 °C for 1 h. The final product was denoted as *x*%Cr-*y*%In/Z, where *x*% and *y*% indicate the weight loadings of Cr and In, respectively, and Z indicated the type of zeolite support. Bimetallic In-containing samples, i.e., Me-In/H-SSZ-13 (Me = Ti, V, Mn, Fe, Co, Ce, Zr, and Mo), were prepared via similar procedures.

2.2. Catalyst characterization

The chemical compositions of samples were analyzed on an IRIS Advantage inductively coupled plasma atomic emission spectrometer.

Transmission electron microscopy (TEM) images of selected samples were acquired on an FEI Tecnai G^2 F20 electron microscope. High-angle annular dark-field scanning transmission electron microscopy (HAADF-STEM) images were acquired on an FEI Talos electron microscope. Element mapping analysis was conducted under HAADF-STEM mode using an FEI built-in energy dispersive spectrum.

X-ray photoelectron spectra (XPS) of samples were acquired on a Thermo Scientific ESCALAB 250Xi spectrometer with a monochromatic Al K_α X-ray source ($h\nu$ = 1486.6 eV). Accurate binding energies (±0.1 eV) were determined with reference to the C 1*s* line of adventitious carbon at 284.8 eV.

The temperature-programmed desorption of ammonia (NH_3-TPD) was performed on a Quantachrome ChemBET 3000 chemisorption analyzer. In a typical experiment, the sample was saturated with 5% NH_3/He at 50 °C and then purged with He at the same temperature for 1 h to eliminate the physical absorbed ammonia. The NH_3-TPD profile was recorded in flowing He at a heating rate of 10 °C/min from 50 to 600 °C.

The experiments of temperature-programmed reduction by hydrogen (H_2-TPR) were also performed on the Quantachrome ChemBET 3000 chemisorption analyzer. In a typical experiment, a sample of 0.1 g was pretreated in 10% O_2/He at 450 °C for 1 h, cooled to 50 °C, and purged for 1 h in flowing He. The H_2-TPR profile was recorded in 5% H_2/Ar (30 mL/min) at a heating rate of 10 °C/min. The outlet gas was passed through a dry-ice trap, and the hydrogen consumption was calculated using CuO as a reference.

2.3. Catalytic study

The CH_4-SCR reaction was performed in a fixed-bed micro-reactor at atmospheric pressure. Typically, a 0.12 mL catalyst sample (20–40 mesh) was placed in a quartz reactor and pretreated in 10% O_2/Ar at 450 °C for 1 h. After cooling to the designated temperature in He, the reactant gas mixture (NO = 2500 ppm; CH_4 = 4000 ppm; O_2 = 4%, H_2O = 6%, He balance) was fed to the catalyst to start the reaction. The total flow rate was set at 150 mL/min resulting in a gas hourly space velocity (GHSV) of 75 000 /h. The outlet gas (H_2O removed by cold trap) was analyzed on-line by a NOx analyzer (Ecotech EC9841) and a gas chromatograph (Techcomp GC7900, equipped with a Plot TDX-1 packed column and an FID detector for the analysis of CH_4 and CO_x, as well as Porapak Q packed column and TCD detector for the analysis of N_2O and N_2). During the reaction, the outlet gas stream was analyzed by a mass spectrometer (Pfeiffer Omnistar GSD 320), and the following mass fragments sensible to the system perturbation were monitored: CH_4 (*m/e* = 15), NO/NO_2 (*m/e* = 30), NO_2 (*m/e* = 46), O_2 (*m/e* = 32), N_2 (*m/e* = 28), CO_2 (*m/e* = 44), NH_3 (*m/e* = 17), H_2O (*m/e* = 18), and HCHO (*m/e* = 29). The NO and CH_4 conversions are defined as follows:

$$\text{NO conversion} = ([NO]_{inlet} - [NO]_{outlet})/[NO]_{inlet} \times 100\%$$

$$\text{NO conversion to } N_2 = 2[N_2]_{outlet}/[NO]_{inlet} \times 100\%$$

$$\text{NO conversion to } NO_2 = [NO_2]_{outlet}/[NO]_{inlet} \times 100\%$$

$$CH_4 \text{ conversion} = ([CH_4]_{inlet} - [CH_4]_{outlet})/[CH_4]_{inlet} \times 100\%$$

$$CH_4 \text{ conversion to } CO_2 = [CO_2]_{outlet}/[CH_4]_{inlet} \times 100\%$$

$$CH_4 \text{ conversion to CO} = [CO]_{outlet}/[CH_4]_{inlet} \times 100\%$$

The temperature-programmed surface reaction (TPSR) of CH_4-SCR was performed on a quartz tube reactor, and the products were analyzed on-line by a Pfeiffer Omnistar GSD 320 mass spectrometer.

3. Results and discussion

3.1. Catalyst characterization

In the representative TEM images of 0.5%Cr/H-SSZ-13 (Fig. 1(a)) and 2%In/H-SSZ-13 (Fig. 1(b)), irregular polygon-like particles with sizes of a dozen nanometers corresponding to the Cr- and In-containing species on the surface of H-SSZ-13 zeolite support can be observed. In contrast, much smaller uniform nanoparticles were distributed on zeolite in the case of 0.5%Cr-2%In/H-SSZ-13 (Fig. 1(c)). From the HAADF-STEM element mapping images (Fig. 1(d) and (e)), the nanoscale aggregations of the Cr and In species can be clearly identified. Meanwhile, the Cr and In species seem to be located in the same regions (marked with white dotted circles), revealing the intimate contact between the Cr and In species. This is further confirmed by a line-scan analysis (red line 1 in Fig. 1(d)) where both the Cr and In species were detected in a single nanoparticle. Since the 0.5%Cr-2%In/H-SSZ-13 sample was submitted to reduction-oxidation treatments at elevated temperatures (see experiment section for details), the Cr and In species should exist in the thermodynamically stable states on H-SSZ-13 support, and the intimate contact between the Cr and In species should originate from their intrinsic properties.

The acidic properties of zeolite catalysts were characterized by means of NH_3-TPD, and the results are shown in Fig. S1. For H-SSZ-13 support, two distinct ammonia desorption peaks were observed corresponding to weak acid sites (peak centered at 200 °C) and strong acid sites (peak centered at 450 °C). The introduction of Cr and/or In to H-SSZ-13 resulted in noticeable decreases in the intensity of strong acid sites because of the interaction of Cr and/or In species with the Brønsted acid sites. Nevertheless, the strong acid sites in parent SSZ-13 zeolite were well preserved after Cr and/or In impregnation and can participate in both methane activation [34] and NO activation [9,14] for CH_4-SCR.

The chemical states of Cr and In species on the zeolite support were investigated by means of XPS. For 0.5%Cr/H-SSZ-13, binding energy peaks at 586.9 ($2p_{1/2}$) and 577.4 ($2p_{3/2}$) eV were observed (Fig. 2(a)) corresponding to the mixture of Cr^{3+}/Cr^{6+} [35,36]. The deconvolution of these peaks was difficult because of the poor signals of Cr with low loading of 0.5%. For 0.5%Cr-2%In/H-SSZ-13, similar binding energy peaks of Cr^{3+}/Cr^{6+} were observed. The difference in the chemical states of Cr in 0.5%Cr/H-SSZ-13 and 0.5%Cr-2%In/H-SSZ-13, even if

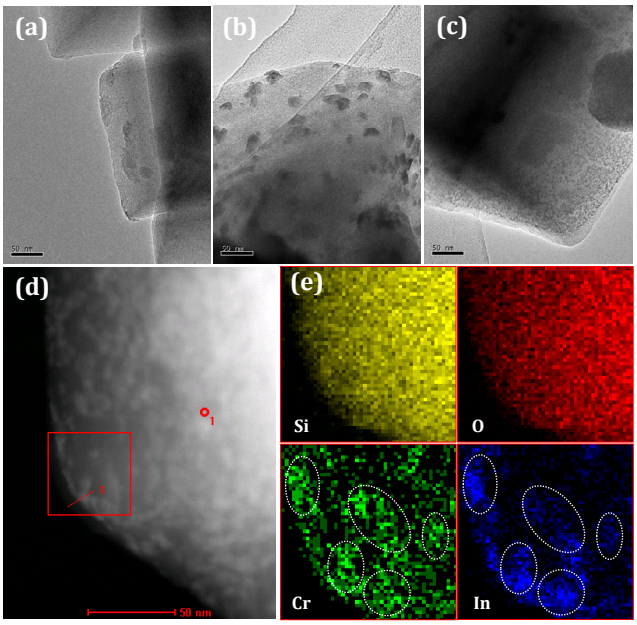

Fig. 1. TEM images of 0.5%Cr/H-SSZ-13 (a), 2%In/H-SSZ-13 (b), 0.5%Cr-2%In/H-SSZ-13 (c); HAADF-STEM image of 0.5%Cr-2%In/H-SSZ-13 (d) with corresponding element mapping (e).

existent, could not be distinguished through XPS analysis. In the In 3*d* XPS, peaks at 453.9 and 446.5 eV were observed for 2%In/H-SSZ-13 attributed to the $3d_{3/2}$ and $3d_{5/2}$ of $(InO)^+$ and/or In_2O_3 species interacting with the zeolite support, respectively [18,37]. For 0.5%Cr-2%In/H-SSZ-13, two additional binding energy value signals at 452.5 and 445.0 eV were clearly observed (Fig. 2(b)). Since the sample was finally oxidized in 10% O_2/Ar at 450 °C, the presence of low-valence In species can be ruled out. In this context, these binding energies should be related to the oxidized In species interacting with the higher-charge density of Cr^{3+}/Cr^{6+}. That is, the electron interaction between the Cr and In species can be revealed by XPS analysis.

The chemical states of the Cr and In species on the zeolite supports were further examined by TPR, and the H_2-TPR profiles are shown in Fig. 3. For 0.5%Cr/H-SSZ-13 (Fig. 3(b)), a series of reduction peaks in the temperature region 250–550 °C were observed corresponding to the reduction of Cr^{6+} to Cr^{3+}

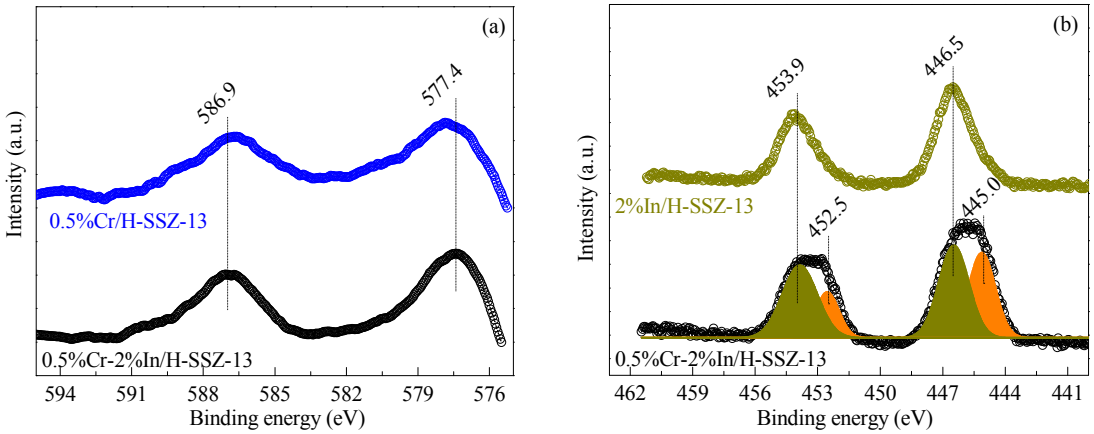

Fig. 2. Cr 2*p* (a) and In 3*d* (b) XPS spectra of 0.5%Cr/H-SSZ-13, 2%In/H-SSZ-13, and 0.5%Cr-2%In/H-SSZ-13.

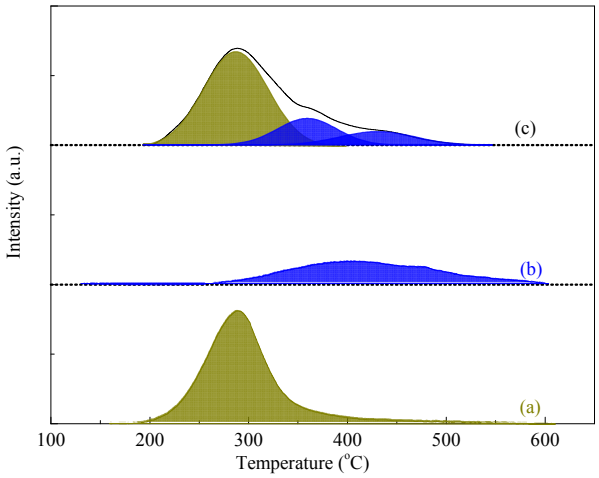

Fig. 3. H_2-TPR profiles of 2%In/H-SSZ-13 (a), 0.5%Cr/H-SSZ-13 (b), and 0.5%Cr-2%In/H-SSZ-13 (c).

and/or Cr^{3+} to Cr^{2+} in different chemical environments [35,38]. The calculated H/Cr ratio was 1.6, confirming the XPS results that a mixture of Cr^{3+}/Cr^{6+} species existed in 0.5%Cr/H-SSZ-13 (Fig. 2). For 2%In/H-SSZ-13 (Fig. 3(a)), a single characteristic reduction peak at 290 °C with a H/In ratio of 1.9 attributed to the reduction of In^{3+} to In^{+} was observed [26]. In the case of bimetallic 0.5%Cr-2%In/H-SSZ-13 (Fig. 3(c)), the reduction of the Cr and In species was well defined: the reduction of the In species was not distinctly affected by the presence of Cr (H/In = 1.8, reduction peak at 290 °C), and the reduction of the Cr species was affected by the presence of In (H/Cr = 1.6, two reduction peaks at 360 and 440 °C). The similar H/In and H/Cr ratios observed for bimetallic 0.5%Cr-2%In/H-SSZ-13 reveal the similar overall average oxidation states of the Cr and In species on the zeolite support with reference to monometallic samples, while the noticeable changes in the reduction peaks corresponding to the Cr species confirms the electron interaction between Cr and In as also revealed by XPS (Fig. 2).

3.2. Catalytic performance of bimetallic Cr-In/H-SSZ-13 in CH_4-SCR

The catalytic performance of 0.5%Cr/H-SSZ-13, 2%In/H-SSZ-13 (optimized In loading employed), and 0.5%Cr-2%In/H-SSZ-13 in the CH_4-SCR reaction was investigated. As shown in Fig. 4, 0.5%Cr/H-SSZ-13 (Fig. 4(a)) exhibited very low activity in the CH_4-SCR reaction (NO conversion to N_2 < 20% at 550 °C), and 2%In/H-SSZ-13 (Fig. 4(b)) exhibited considerable activity (NO conversion to N_2 > 40% at 550 °C). The physical mixture of 0.5%Cr/H-SSZ-13 (0.12 mL) and 2%In/H-SSZ-13 (0.12 mL) (Fig. 4(c)) appeared to be more ac-

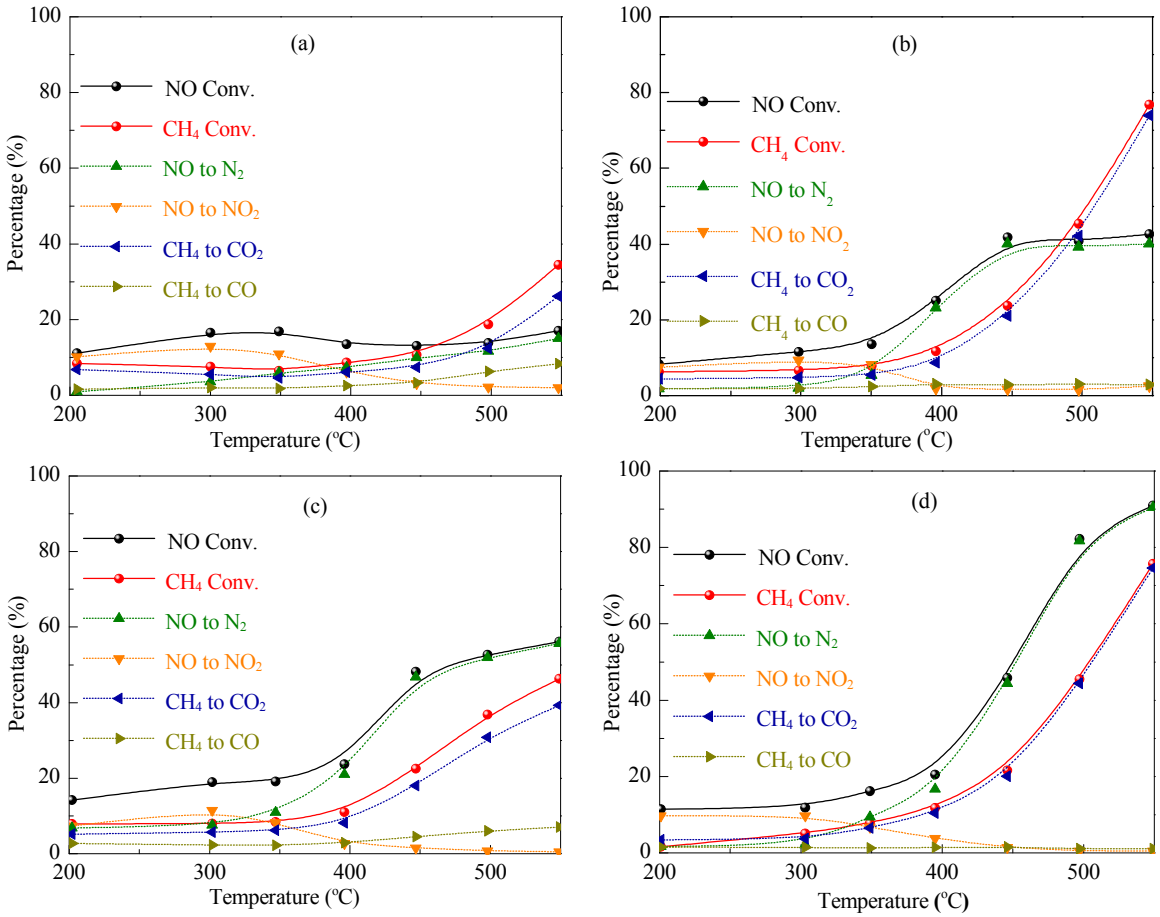

Fig. 4. CH_4-SCR over 0.5%Cr/H-SSZ-13 (a), 2%In/H-SSZ-13 (b), physical mixture of 0.5%Cr/H-SSZ-13 and 2%In/H-SSZ-13 (c), and 0.5%Cr-2%In/H-SSZ-13 (d). Reaction conditions: 2500 ppm NO, 4000 ppm CH_4, 4% O_2, 6% H_2O, He balance; GHSV = 75 000 /h.

tive, but it acted more like a simple accumulation of two individual components. In contrast, bimetallic 0.5%Cr-2%In/H-SSZ-13 (Fig. 4(d)) was very active in the CH_4-SCR reaction. Typically, NO conversion increased from 10% to more than 90% with an increasing reaction temperature from 300 to 550 °C, and N_2 selectivity greater than 99% was obtained at temperatures greater than 450 °C. Obviously, a cooperative effect between the Cr and In species did exist and played a key role in the CH_4-SCR reaction catalyzed by bimetallic 0.5%Cr-2%In/H-SSZ-13. In other words, the presence of Cr dramatically promoted the CH_4-SCR reaction over In/H-SSZ-13.

The catalytic performance of bimetallic Cr-In on different supports was investigated. As shown in Fig. 5, the support materials played a decisive role in the CH_4-SCR activity of the Cr-In catalysts. H-SSZ-13 appears to be the best support for the Cr-In active species, followed by H-ZSM-5. H-beta and SiO_2 are not suitable support materials, and very low CH_4-SCR activity was observed for Cr-In/H-beta and Cr-In/SiO_2. H-SSZ-13 can be clearly optimized from all the support materials investigated. An extra advantage of using H-SSZ-13 as support is its remarkable thermal and hydrothermal stability, which should be good for the catalytic stability of 0.5%Cr-2%In/H-SSZ-13 at elevated temperatures and in the presence of excess H_2O (vide infra).

A series of bimetallic In-containing zeolite catalysts were further applied in the CH_4-SCR reaction to elaborate the unique promotion effect of the Cr species. As shown in Fig. 6, some elements, i.e., Fe, V, Mo, Cr, Ce, and Co show promotion effects on In/H-SSZ-13 for the CH_4-SCR reaction, while others (Ti, Mn, and Zr) do not. It has been reported that Ce [20] and Co [3,19] can significantly promote the CH_4-SCR reaction over In/zeolites, and similar promotion effects were observed here. Fortunately, the best promotion effect of Cr on In/H-SSZ-13 for CH_4-SCR was disclosed for the first time in this study. To our knowledge, bimetallic 0.5%Cr-2%In/H-SSZ-13 appears to be the most active CH_4-SCR catalysts under comparable reaction conditions, i.e., high NO inlet concentration, high GHSV, and excessive H_2O [3,10,14,30,39]. For bimetallic *x*%Cr-2%In/H-SSZ-13 catalysts, increasing the Cr loading from 0.2% to 0.5% showed noticeable positive impacts on the CH_4-SCR activity, while further increases of Cr loading to 1% had no significant effect (Fig. S2).

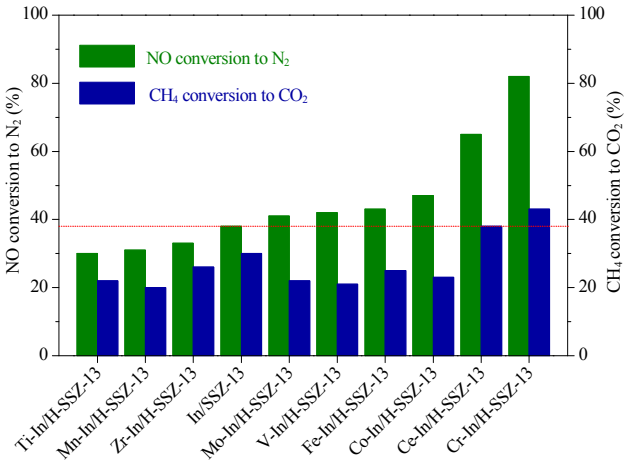

Fig. 6. Comparison of In-based bimetallic catalysts supported on H-SSZ-13 for CH_4-SCR. Reaction conditions: 2500 ppm NO, 4000 ppm CH_4, 4% O_2, 6% H_2O, He balance; T = 500 °C; GHSV = 75 000 /h.

Some reaction parameters, e.g., space velocity (Fig. S3) and O_2 and CH_4 concentration in feeding gas (Fig. S4), were also investigated. In the absence of O_2, relatively low NO conversion to N_2 was observed above 300 °C, which should come from the direct decomposition of NO (Eq. (4)). The introduction of O_2 to the reaction system can help to activate NO and/or CH_4, and, therefore, trigger the CH_4-SCR reaction [39,40]. More O_2 can slightly promote NO oxidation below 300 °C and CH_4 oxidation at temperatures greater than 400 °C. In this study, excess CH_4 was employed for NO (Eq. (1)) since CH_4 is cheap and easily available in natural gas power plants and the unreacted CH_4 can be removed by catalytic combustion (Eqs. (2) and (3)). As expected, changing the CH_4 concentration within the range 3000–5000 ppm did not significantly influence the CH_4-SCR activity, while the efficiency of the CH_4 reducing agent differed slightly (Fig. S4).

According to our experimental observations and literature reports [4,23], the possible reactions during CH_4-SCR are iden-

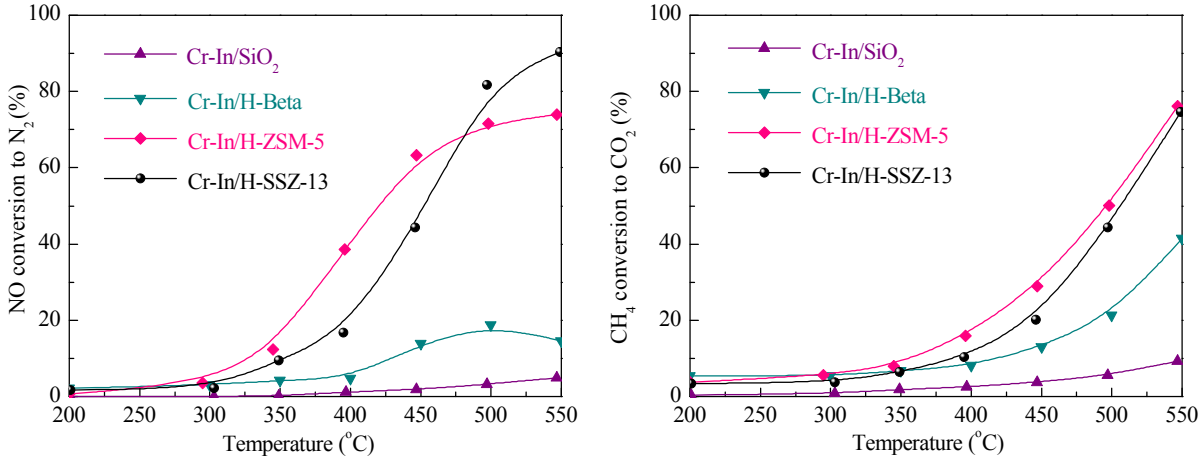

Fig. 5. CH_4-SCR over 0.5%Cr-2%In/SiO_2, 0.5%Cr-2%In/H-ZSM-5, 0.5%Cr-2%In/H-beta, and 0.5%Cr-2%In/H-SSZ-13 (Si/Al = 25). Reaction conditions: 2500 ppm NO, 4000 ppm CH_4, 4% O_2, 6% H_2O, He balance; GHSV = 75 000 /h.

tified below:

$$2NO + CH_4 + O_2 \rightarrow N_2 + 2H_2O + CO_2 \quad (1)$$

$$CH_4 + 2O_2 \rightarrow 2H_2O + CO_2 \quad (2)$$

$$2CH_4 + 3O_2 \rightarrow 4H_2O + 2CO \quad (3)$$

$$2NO \rightarrow N_2 + O_2 \quad (4)$$

$$2NO + O_2 \rightarrow 2NO_2 \quad (5)$$

$$2CO + 2NO \rightarrow N_2 + 2CO_2 \quad (6)$$

Among these reactions, CH_4 oxidation to CO_2 or CO by O_2 (Eqs. (2) and (3)) and NO oxidation to NO_2 by O_2 (Eq. (5)) are known as major side reactions. However, they are related to the activation of CH_4 and NO, respectively, and show significant impacts on CH_4-SCR. Therefore, the reactions catalyzed by 0.5%Cr/H-SSZ-13, 2%In/H-SSZ-13, and 0.5%Cr-2%In/H-SSZ-13 were investigated. As shown in Fig. S5, noticeable NO oxidation to NO_2 with maximal NO conversion of 25% was achieved in the temperature range 200–450 °C over all three catalysts. Obviously, Cr does not significantly promote the oxidation of NO to gaseous NO_2. Moreover, the gas-phase NO_2 formation is not the rate-determining step in CH_4-SCR since the CH_4-SCR rate is apparently higher than that of NO oxidation (Figs. 4 and S5).

For CH_4 oxidation, 0.5%Cr/H-SSZ-13 exhibited relatively low activity and a considerable amount of CO was produced from incomplete oxidation (Fig. S6). 2%In/H-SSZ-13 exhibited moderate activity in CH_4 oxidation, with CO_2 as the dominating product. 0.5%Cr-2%In/H-SSZ-13 appeared to be more active than 0.5%Cr/H-SSZ-13 and 2%In/H-SSZ-13, and the formation of CO as observed in the case of 0.5%Cr/H-SSZ-13 was significantly suppressed. These observations indicate the cooperation between Cr and In during CH_4 oxidation. It has been claimed that CH_4 oxidation competes with CH_4-SCR, especially at high temperatures, and higher CH_4 oxidation activity may lead to lower CH_4-SCR activity [41]. However, CH_4 oxidation activity may indicate the capability of CH_4 activation, which is also very important for CH_4-SCR. Since excess CH_4 was employed in the CH_4-SCR in this study, higher CH_4 oxidation activity correlates with higher CH_4-SCR activity (Figs. 4 and S6).

The stability of 0.5%Cr-2%In/H-SSZ-13 during CH_4-SCR at 500 °C was investigated. As shown in Fig. 7, NO conversion to N_2 over 0.5%Cr-2%In/H-SSZ-13 was very stable for the first 30 h of the CH_4-SCR reaction in the absence of H_2O (NO conversion of 84%). The introduction of 6% H_2O to the reaction system caused a slight decrease in NO conversion to 82%, which was stable for the next 90 h. After the feeding of H_2O was stopped, the NO conversion gradually recovered to the initial value and remained at this level for a further 30 h. These observations indicate that the presence of excess H_2O shows reversible negative impacts on CH_4-SCR, probably by competing adsorption on the active sites. The remarkable catalytic stability of 0.5%Cr-2%In/H-SSZ-13 can be explained from the stability of both the bimetallic active centers and the zeolite support. Through reduction-oxidation treatment, bimetallic Cr-In species exist in the thermodynamically stable states and their structures during reaction will not change. Meanwhile, H-SSZ-13 zeolite was very stable upon thermal and hydrothermal treatments, and the structure destruction because of the framework dealumination was completely suppressed. On the whole, 0.5%Cr-2%In/H-SSZ-13 appears to be an eligible CH_4-SCR catalyst for potential applications.

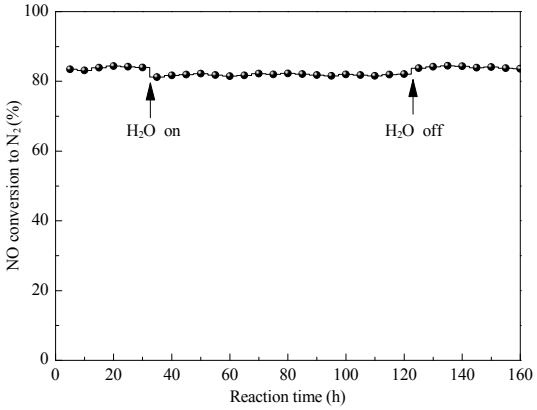

Fig. 7. Stability test of 0.5%Cr-2%In/H-SSZ-13 in CH_4-SCR. Reaction conditions: 2500 ppm NO, 4000 ppm CH_4, 4% O_2, 0 or 6% H_2O, He balance; T = 500 °C; GHSV = 75 000 /h.

3.3. Reaction intermediate

The reaction intermediates in CH_4-SCR were investigated by means of TPSR, and the results are shown in Fig. 8. The activity difference in CH_4-SCR was well identified and in good agree-

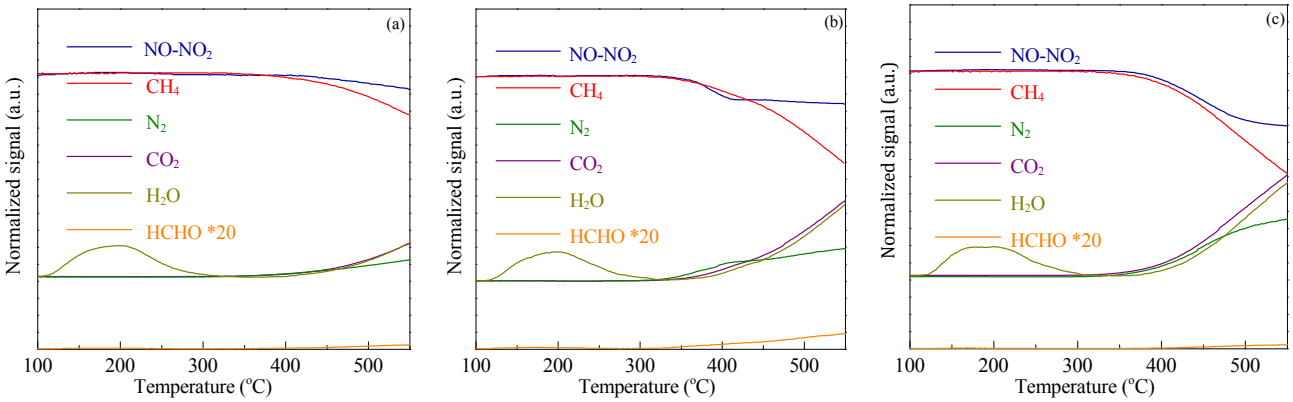

Fig. 8. TPSR of CH_4-SCR over 0.5%Cr/H-SSZ-13 (a), 2%In/H-SSZ-13 (b), and 0.5%Cr-2%In/H-SSZ-13 (c). Reaction conditions: 0.1 g catalyst, 2500 ppm NO, 4000 ppm CH_4, 4% O_2, He balance; total flow rate = 100 mL/min.

ment with the steady-state reaction results (Fig. 4). Formaldehyde (HCHO) from the incomplete oxidation of methane was detected as the exclusive carbon-containing intermediate gaseous product during CH_4-SCR over 2%In/H-SSZ-13, indicating the oxidative activation of CH_4 to HCHO over the In species. The further oxidation of HCHO (by O_2, NO, NO_2, or other oxidants) to H_2O and CO_2 was apparently a slow step over 2%In/H-SSZ-13. While in the case of 0.5%Cr-2%In/H-SSZ-13, the formation of HCHO was greatly suppressed and a rational explanation is that the further oxidation of HCHO was promoted by the presence of the Cr species. Another interesting phenomenon is that the conversion of NO/NO_2 to N_2 was faster than the CH_4 conversion to CO_2 over 2%In/H-SSZ-13 (Fig. 8(b)), hinting to a mechanism of NO decomposition followed by oxygen removal. In contrast, a synchronous conversion of NO/NO_2 and CH_4 was observed over bimetallic 0.5%Cr-2%In/H-SSZ-13 (Fig. 8(c)). According to the TPSR results, we propose that the activation of NO occurs on Cr species, while the activation of CH_4 occurs on In species. The cooperation between Cr and In species is responsible for the remarkable CH_4-SCR activity of 0.5%Cr-2%In/H-SSZ-13 in accordance with the steady-state reaction results.

4. Conclusions

Bimetallic 0.5%Cr-2%In/H-SSZ-13 was successfully developed as a robust catalyst for CH_4-SCR, outperforming monometallic Cr/H-SSZ-13, In/H-SSZ-13, and their mixture. Typically, NO conversion greater than 90% with N_2 selectivity greater than 99% was achieved at 550 °C and high GHSV of 75 000 /h in the presence of 6% H_2O. Through reduction-oxidation treatments, Cr and In species existed in the thermodynamically stable states on H-SSZ-13. TEM images and XPS results revealed a close contact between Cr and In species as well as their interaction, which is helpful for constructing an efficient cooperative catalysis system. According to the catalytic data, the activation of CH_4 and NO occurred on the In and Cr sites of bimetallic Cr-In/H-SSZ-13, respectively, both with the participation of O_2.

Supporting Information

More characterization results and catalytic results in CH_4-SCR.

References

[1] European Environment Agency, *Nitrogen Oxides (NO_x) Emissions*. **2010**, 1–20.
[2] F. Lónyi, H. E. Solt, Z. Pászti, J. Valyon, *Appl. Catal. B*, **2014**, 150–151, 218–229.
[3] F. Lónyi, H. E. Solt, J. Valyon, A. Boix, L. B. Gutierrez, *Appl. Catal. B*, **2012**, 117–118, 212–223.
[4] J. N. Armor, *Catal. Today*, **1995**, 26, 147–158.
[5] N. W. Cant, I. O. Y. Liu, *Catal. Today*, **2000**, 63, 133–146.
[6] J. A Loiland, R. F. Lobo, *J. Catal.*, **2015**, 325, 68–78.
[7] M. Wallin, C. J. Karlsson, M. Skoglundh, A. Palmqvist, *J. Catal.*, **2003**, 218, 354–364.
[8] S. A. Stevenson, J. C. Vartuli, C. F. Brooks, *J. Catal.*, **2000**, 190, 228–239.
[9] R. D. Zhang, N. Liu, Z. G. Lei, B. H. Chen, *Chem. Rev.*, **2016**, 116, 3658–3721.
[10] A. N. Mendes, V. L. Zholobenko, F. Thibault-Starzykc, P. Da Costa, C. Henriques, *Appl. Catal. B*, **2016**, 195, 121–131.
[11] I. O. Costilla, M. D. Sanchez, M. A. Volpe, C. E. Gigola, *Catal. Today*, **2011**, 172, 84–89.
[12] J. A. Z. Pieterse, S. Booneveld, *Appl. Catal. B*, **2007**, 73, 327–335.
[13] H. Decolatti, H. Solt, F. Lónyi, J. Valyon, E. Miró, L. Gutierrez, *Catal. Today*, **2011**, 172, 124–131.
[14] F. Lónyi, H. E. Solt, J. Valyon, H. Decolatti, L. B. Gutierrez, E. Miró, *Appl. Catal. B*, **2010**, 100, 133–142.
[15] L. Gutierrez, A. Boix, J. O. Petunchi, *J. Catal.*, **1998**, 179, 179–191.
[16] F. Lonyi, J. Valyon, L. Gutierrez, M. A. Ulla, E. A. Lombardo, *Appl. Catal. B*, **2007**, 73, 1–10.
[17] L. Gutierrez, E. A. Lombardo, *Appl. Catal. A*, **2009**, 360, 107–119.
[18] H. P. Decolatti, E. G. Gioria, S. N. Ibarlín, N. Navascues, S. Irusta, E. E. Miro, L. B. Gutierrez, *Microporous Mesoporous Mater.*, **2016**, 222, 9–22.
[19] F. Lónyi, H. E. Solt, J. Valyon, A. Boix, L. B. Gutierrez, *J. Mol. Catal. A*, **2011**, 345, 75–80.
[20] T. Sowade, T. Liese, C. Schmidt, F. W. Schütze, X. Yu, H. Bernd, W. Grünert, *J. Catal.*, **2004**, 225, 105–115.

Graphical Abstract

Chin. J. Catal., 2018, 39: 1004–1011 doi: 10.1016/S1872-2067(18)63054-2

Bimetallic Cr-In/H-SSZ-13 for selective catalytic reduction of nitric oxide by methane

Jun Yang, Yupeng Chang, Weili Dai, Guangjun Wu, Naijia Guan, Landong Li *
Nankai University

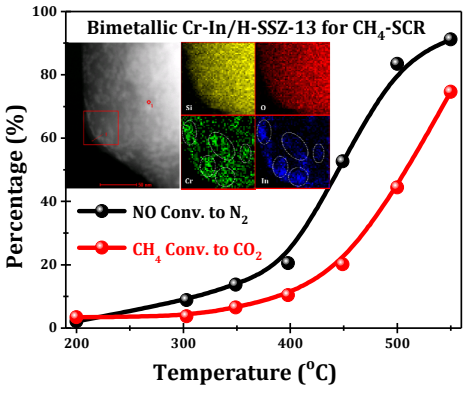

The bimetallic Cr-In/H-SSZ-13 catalyst exhibited appreciable reactivity and hydrothermal stability in the CH_4-SCR process.

[21] R. Serra, M. J. Vecchietti, E. Miro, A. Boix, *Catal. Today*, **2008**, 133–135, 480–486.
[22] H. Pan, Y. F. Jian, Y. K. Yu, N. N. Chen, C. He, C. He, *Appl. Surf. Sci.*, **2016**, 390, 608–616.
[23] T. Maunula, J. Ahola, H. Hamada, *Appl. Catal. B*, **2006**, 64, 13–24.
[24] J. M. Zamaro, M. A. Ulla, E. E. Miro, *Catal. Today*, **2005**, 107–108, 86–93.
[25] O. A. Anunziata, A. R. Beltramone, F. G. Requejo, *J. Mol. Catal. A*, **2007**, 267, 194–201.
[26] E. E. Miro, L. Gutierrez, J. M. R. Lopez, F. G. Requejo, *J. Catal.*, **1999**, 188, 375–384.
[27] M. Ogura, T. Ohsaki, E. Kikuchi, *Microporous Mesoporous Mater.*, **1998**, 21, 533–540.
[28] X. J. Zhou, Z. S. Xu, T. Zhang, L. W. Lin, *J. Mol. Catal. A*, **199**7, 122, 125–129.
[29] E. Kikuchi, M. Ogura, I. Terasaki, Y. Goto, *J. Catal.*, **1996**, 161, 465–470.
[30] M. C. Campa, D. Pietrogiacomi, M. Occhiuzzi, *Appl. Catal. B*, **2015**, 168–169, 293–302.
[31] S. W. Chen, X. L. Yan, J. Q. Chen, J. H. Ma, R. F. Li, *Chin. J. Catal.*, **2010**, 31, 1107–1114.
[32] T. Tabata, M. Kokitsu, O. Okada, *Appl. Catal. B*, **1995**, 6, 225–236.
[33] Y. J. Li, T. L. Slager, J. N. Armor, *J. Catal.*, **1994**, 150, 388–399.
[34] V. L. Sushkevich, D. Palagin, M. Ranocchiari, J. A. van Bokhoven, *Science*, **2017**, 356, 523–527.
[35] F. Ayari, M. Mhamdi, J. Alvarez-Rodriguez, A. R. G. Ruiz, G. Delahay, A. Ghorbel, *Appl. Catal. B*, **2013**, 134–135, 367–380.
[36] F. Ayari, M. Mhamdi, T. Hammedia, J. Alvarez-Rodriguez, A.R.G. Ruiz, G. Delahay, A. Ghorbel, *Appl. Catal. A*, **2012**, 439–440, 88–100.
[37] J. M. Zamaro, E. E. Miro, A. V. Boix, A. Martínez-Hernandez, G. A. Fuentes, *Microporous Mesoporous Mater.*, **2010**, 129, 74–81.
[38] A. Hakuli, M. E. Harlin, L. B. Backman, A. O. I. Krause, *J. Catal.*, **1999**, 184, 349–356.
[39] M. Takahashi, T. Nakatani, S. Iwamoto, T. Watanabe, M. Inoue, *Appl. Catal. B*, **2007**, 70, 73–79.
[40] S. B. Xie, M. P. Rosynek, J. H. Lunsford, *J. Catal.*, **1999**, 188, 32–39.
[41] T. Nakatani, T. Watanabe, M. Takahashi, Y. Miyahara, H. Deguchi, S. Iwamoto, H. Kanai, M. Inoue, *J. Phys. Chem. A*, **2009**, 113, 7021–7029.

双金属 Cr-In/H-SSZ-13 催化剂上 CH_4 选择催化还原 NO

杨 俊[a], 常煜鹏[a], 戴卫理[a], 武光军[a], 关乃佳[a,b], 李兰冬[a,b,*]
[a]南开大学材料科学与工程学院, 国家新材料研究院, 天津 300350
[b]南开大学先进能源材料化学教育部重点实验室, 化学化工协同创新中心, 天津 300071

摘要: 天然气 (主要成分为甲烷) 储量丰富, 价格低, 随着国内电厂煤改气的进行, 甲烷作为还原剂选择催化还原氮氧化物成为电厂烟气脱硝的理想选择, 受到广泛关注. In 改性分子筛催化剂在甲烷选择催化还原一氧化氮反应 (CH_4-SCR) 中表现出一定催化性能, 而 In 基双金属被认为是最有前景的 CH_4-SCR 催化剂. 本文通过湿浸渍法制备了分子筛双金属催化剂, 并成功应用于CH_4-SCR. 我们首先研究了不同分子筛载体、助剂及含量、氧气浓度、甲烷浓度和空速对反应的影响, 发现 0.5%Cr-2%In/H-SSZ-13 在 CH_4-SCR中表现出最佳的催化性能: NO 转化率 > 90%, N_2选择性 > 99% (反应条件: 550 °C, 6% H_2O, 空速 75 000 /h). 从透射电镜照片可以看出, 0.5%Cr-2%In/H-SSZ-13催化剂上均匀分布纳米尺寸颗粒, 扫描透射-高角环形暗场像元素分布分析表明 Cr 与 In 出现在同一个位置, 即 Cr 与 In 紧密接触. X射线光电子能谱结果表明, 与单金属催化剂相比, 双金属催化剂中 In 的能谱发生了明显偏移, Cr 与 In 存在电子相互作用. CH_4-SCR 反应活性实验发现, 双金属催化剂活性远远超过单金属催化剂活性及其机械混合物, 表明 Cr 的添加可以明显促进 In 的活性. 换言之, 双金属催化剂中, Cr 与 In 存在协同催化作用. Cr-In/H-SSZ-13在严苛反应条件下的活性长期保持不变, 具有良好稳定性, 这与沸石分子筛载体 H-SSZ-13 的高热稳定性分不开. 结合稳态反应与程序升温表面反应结果, 可以推测有氧条件下 CH_4 和 NO 分别在 In 和 Cr 位点上活化.

关键词: 选择催化还原; 一氧化氮; 甲烷; Cr-In/H-SSZ-13; 双金属催化剂

收稿日期: 2018-02-07. 接受日期: 2018-03-07. 出版日期: 2018-05-05.
*通讯联系人. 电话/传真: (022)23500341; 电子信箱: lild@nankai.edu.cn
基金来源: 国家自然科学基金 (21773127, 21722303, 21421001); 高等学校学科创新引智计划 (111计划, B18030).
本文的电子版全文由Elsevier出版社在ScienceDirect上出版(http://www.sciencedirect.com/science/journal/18722067).